RSC Advances

PAPER

View Article Online
View Journal | View Issue

Cite this: *RSC Adv.*, 2024, **14**, 24952

Waste bamboo-derived magnetically separable bamboo-activated carbon: from characterization to effective remediation of fluoride (F^-) ions from water†

Yana Bagbi, *[a] Pokjum Yomgam,[ac] Enuk Libang,[ac] Bijoylakshmi Boruah,[ad] Jaspreet Kaur,[b] S. Jayanthi,[d] Sanjeev Kumar[c] and Narender K. Dhania *[b]

An effective and affordable nanoadsorbent, magnetically separable magnetite-activated bamboo carbon (MABC), was obtained from waste bamboo biomass *via* pyrolysis of bamboo chunks and the co-precipitation method using ferrous and ferric chloride as iron precursors. The synthesized nanosorbents were characterised using XRD, SEM, and DLS techniques to study the surface characteristics and morphology. Chemical composition, optical absorption, and magnetic properties were studied using FTIR spectroscopy, UV-vis spectroscopy, and VSM, respectively. The BET surface area, porosity and surface charge were determined using N_2 adsorption–desorption isotherm and zeta potential technique. The cytotoxicity and antimicrobial properties of BC, ABC and MABC were investigated against prokaryotes and eukaryotes. The result demonstrates the nontoxic nature of BC, ABC and MABC, indicating their significant potential for addressing water treatment using sustainable and eco-friendly nanosorbents. Comparative fluoride ion removal studies were performed using ABC and MABC NPs. About 99.6% of F^- ions were adsorbed using MABC and 75.9% were adsorbed using ABC. Thus, MABC NPs were used as sorbents for the rest of the fluoride ion adsorption parameters. The batch fluoride ion sorption was performed at various sorption parameters, such as diverse solution pH (1.0–8.0), temperature (25–45 °C), agitation times (10–60 min), and adsorbent dose (0.01–0.04 g L^{-1}). The pseudo-second-order kinetic model exhibited the best fit with F^- ion adsorption (95.96 mg g^{-1}) compared with the pseudo-first-order model (12.30 mg g^{-1}), thereby indicating chemisorption adsorption. The exhausted MABC was recovered from the aqueous solution using a bar magnet. Regeneration studies of exhausted MABC were successfully performed using NaOH (0.1 M) as a desorbing agent.

Received 21st May 2024
Accepted 25th July 2024

DOI: 10.1039/d4ra03752a

rsc.li/rsc-advances

1. Introduction

Water pollution is a growing environmental concern, with contaminants such as heavy metals and minerals posing significant risks to public health and aquatic ecosystems.[1,2] Water pollution arises from various anthropogenic activities, including industrial discharges, agricultural runoff, municipal wastewater, and improper waste disposal.[2]

Fluoride is a naturally occurring mineral from rocks in groundwater and surface water sources. It can also be introduced into the water through industrial processes and fluoridated compounds used for public health benefits. In groundwater, a high concentration of fluoride (F^-) ions is due to the weathering of fluorspars (CaF_2), cryolite (Na_3AlF_6), and fluorapatite [$Ca_5(PO_4)_3F$] present in the earth's crusts.[3,4] It is also due to the volcanic and fumarolic processes.[3,4] Fluoride benefits dental health in controlled concentrations of up to 1.0 mg L^{-1}. However, excessive fluoride levels in drinking water can lead to health problems such as oral health (dental fluorosis and skeletal fluorosis poisoning), bone damage, osteoporosis, joint-related issues, and damage to the heart, kidney, liver, neuron system, arteries, endocrine glands, and several other delicate parts of a living organism.[3,4] WHO (World Health Organization) and BIS (Bureau of Indian Standards) have fixed the maximum permissible limit of fluoride as 1.5 mg L^{-1} in potable water.[5,6] Globally, high fluoride concentrations in groundwater have

[a]*Department of Physics & Astrophysics, University of Delhi, 110007, India. E-mail: yanabagbi@gmail.com*

[b]*Department of Zoology, Faculty of Sciences, University of Delhi, 110007, India. E-mail: narender@zoology.du.ac.in*

[c]*Department of Physics, Rajiv Gandhi University, Doimukh, Arunachal Pradesh-791109, India*

[d]*Department of Physics, Jawaharlal Nehru College, Pasighat, Arunachal Pradesh-791103, India*

† Electronic supplementary information (ESI) available. See DOI: https://doi.org/10.1039/d4ra03752a

been reported in China, the United States, Canada, Mexico, South Korea, Australia, Yemen, Turkey, Saudi Arabia, Indonesia, Iran, Pakistan, Sri Lanka, and India.[7,8]

In India, it is reported that fluoride contamination in water was found in Assam, Rajasthan, Gujarat, Uttar Pradesh, Andhra Pradesh, Haryana, Karnataka, Jharkhand, Madhya Pradesh, *etc.*[8,9] Therefore, removing excessive fluoride ions from water ensures safe drinking water supplies.

Water DE-fluoridation methods include adsorption, ion exchange, precipitation, and reverse osmosis. Adsorbents such as bone char, activated alumina, aluminium-impregnated carbon, activated alumina, alum-impregnated activated alumina, activated carbons, carbon black, red mud, zeolite, chitin, chitosan, magnetic-chitosan particle, limestone, and carbonaceous materials were reported.[8,10] Most of the developed adsorbents are tested only under laboratory conditions. Thus, there is an urgent need to create a tailor-made, low-cost, sustainable technology for fluoride removal.

Water purification using carbon-based materials such as activated carbon adsorbents is widely used to remove fluoride ions from water because they show high selectivity, well-developed internal pore structure, simple operation, and large surface area.[11,12] Nonetheless, commercially available activated carbon does encounter specific issues, including relatively high expenses, limited adsorption capacity, and poor renewability, which have hindered its widespread adoption in water treatment.[13–15] Therefore, various technologies, including physical, chemical, and physicochemical methods, have been developed in recent years to enhance the utilisation value of activated carbon.[14,15] Among these methods, chemical activation is widely used to prepare activated carbon. The choice of activating reagents is crucial in developing porous structures, along with choosing suitable functional groups for the surface of the materials.[11,12] However, these methods often involve using expensive chemicals and generating sludge or hazardous waste, and they may need to be more environmentally sustainable in the long run.[14]

Recently, with these drawbacks and the intention of achieving enhanced economic viability, research has shifted its focus toward utilising inexpensive and renewable carbonaceous materials for active carbon production.[14,15] Such materials include rice husks, coconut shells, bones, industrial by-products, waste bamboo (*Bambusa vulgari*) and many more.[16–18] Parameters such as their textural characteristics and surface chemistry influence the adsorption capacity of adsorbents. There has been increasing interest in sustainable and cost-effective alternatives for fluoride removal, and one promising solution is the use of various locally available carbonaceous agricultural waste plant biomasses, such as bamboo, to produce activated bamboo carbon.[17,18]

In this view, activated bamboo carbon derived from waste bamboo has emerged as an invaluable source for water purification (drinking water, Sewage, and industrial water treatment) due to its highly developed porosity, large surface area, highly variable surface chemistry, biodegradability, environmentally friendly, biocompatibility, renewability, and high electric conductivity.[19–22] Various studies have reported that bamboo charcoal is a promising adsorbent for eliminating metal ions, dyes, pesticides, and phenols.[19–22] It is widely used in water purification, air purification, gas purification, chromatographic separation, agricultural feedstock, wastewater treatment, *etc.*[19–22]

Bamboo is a fast-growing, environmentally friendly, plentiful, renewable woody plant bio-resource.[22,23] Bamboo has moderately high carbon content (48.64%) and low amounts of nitrogen (0.14%), sulfur (0.11%) and hydrogen (6.75%).[24] Carbon obtained from bamboo is rich in minerals, including magnesium, calcium, potassium, and sodium.[22,24] Using it as a filter increases drinking water quality because its minerals are dissolved in water. Compared with modern carbon filters, bamboo carbon has the added benefit of a built-in team of microbes working on decomposing toxic substances; hence, the water is clear of harmful substances, yeasts, and microbes.[25] Carbon obtained from bamboo releases a type of electromagnetic wave called Far Infrared Waves (FIR) at wavelengths ranging from 4 to 16 micrometres. Besides, bamboo charcoal purifies the water by adsorbing harmful dyes and acts as a disinfectant for waterborne germs.[24,26]

Recently, magnetic separation has turned out to be the most favourable method for environmental purification because it yields no contamination and is easily detached from the water medium under the applied magnetic field.[27–29] Hence, activated carbon from bamboo with magnetic properties has become a new class of intelligent materials that has attracted interest as absorbents to remove toxic materials from the aquatic media using bar magnets.[8,27]

In this study, activated bamboo carbon (ABC) was derived from bamboo waste biomass as the source. Afterwards, ABC was magnetised by grafting magnetite nanoparticles into it to develop magnetite-activated bamboo carbon (MABC), which improves the specific adsorption capacity and expands the scope of its utilisation in water research. Grafting magnetite nanoparticles into activated carbon can easily separate the adsorbents from water and reuse them for further sorption analysis. The physical and chemical characteristics of synthesised BC, ABC and MABC were studied and analysed using various techniques. Various studies have reported that nanoparticles have toxic and inflammatory effects on living cells. Thus, cytotoxicity and antibacterial analysis of BC, ABC and MABC NPs were examined against both prokaryotes and eukaryotes. Batch adsorption studies have been performed at multiple sorption parameters, such as diverse solution pH (1.0–8.0), temperature (25–45 °C), contact times (10–60 min), and adsorbent dose (0.01–0.04 g L^{-1}). The 5-cycle desorption studies were performed to regenerate exhausted MABC using HNO_3 (0.005 M) as a desorbing agent.

2. Materials and methods

The following chemicals and reagents, such as ferrous chloride tetrahydrate ($FeCl_2 \cdot 4H_2O$) from SRL, iron(III) chloride ($FeCl_3$) anhydrous from Merck life, sodium fluoride (NaF), sodium hydroxide pellets (NaOH) from SRL, ethanol (C_2H_5OH) from Supelco and nitric acid (HNO_3) from SRL, were used for the

synthesis. Waste bamboo chunks were collected from the bamboo market in Itanagar, Arunachal Pradesh, India.

2.1 Synthesis of adsorbents BC, ABC and MABC NPs

Three significant phases are required to obtain MABC NPs. (a) Synthesis of bamboo carbon (BC), (b) activation of bamboo carbon (ABC), and (c) magnetite-activated bamboo carbon (MABC).

2.1.1 Preparation of bamboo carbon (BC). First, locally available waste bamboo chunks were collected from the bamboo market in Itanagar, Arunachal Pradesh, and cut into small pieces called bamboo slices. Then, it was washed several

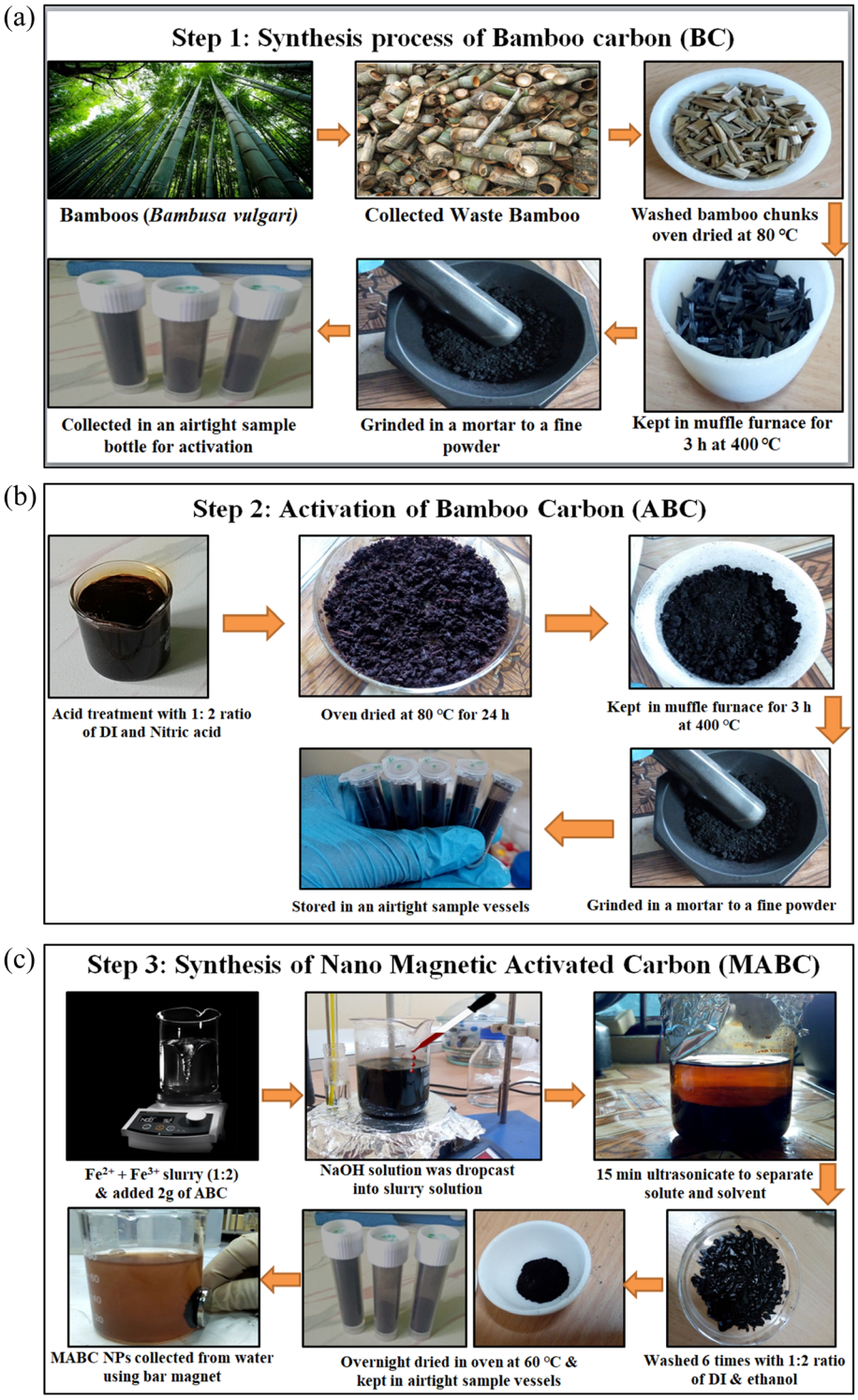

Fig. 1 (a) Image showing the synthesis process of bamboo carbon (BC). (b) Image showing the activation process of bamboo carbon (ABC). (c) Image showing nano-magnetite-activated bamboo carbon (MABC NPs).

times with distilled water and acetone to remove dirt and was oven-dried at 80 °C for 8 h. Washed and dried bamboo chunks were pyrolysed at 400 °C (300–600 °C, depending on the size of the bamboo) for 3 h in a temperature-controlled muffle furnace. The obtained bamboo carbon was ground in a mortar into a fine powder. The resultant powdered bamboo carbon (BC) was kept in an airtight sample vessel and further used for BC activation. The detailed synthesis process of bamboo carbon (BC) is shown in Fig. 1(a).

2.1.2 Preparation of activated bamboo carbons (ABCs). Activating carbonised bamboo carbon is essential for improving the original structure and increasing the adsorption properties. Prepared powdered bamboo carbon (2 g) was activated by the treatment of nitric acid (HNO_3) and distilled water in a ratio of 1 : 2 (2.25 mL HNO_3 : 4.5 mL DI). The paste was oven-dried at 80 °C for 24 h and placed in a muffle furnace for 3 h at a temperature of 400 °C. The obtained activated bamboo carbon (ABC) (resembling tea powder) was ground finely. The final ground products were rinsed with distilled water several times until the pH was obtained at 6.0 and used for further examination. Fig. 1(b) shows the activation process of bamboo carbon to obtain ABC.

2.1.3 Preparation of nano-magnetite-activated bamboo carbon (MABC). First, 2 g of prepared powdered activated bamboo carbon (ABC) was suspended in 100 mL of distilled water. The magnetite suspension was precipitated by mixing ferric and ferrous solutions at a molar ratio of 1 : 2. First, a solution of ferrous chloride was freshly prepared by dissolving 3.97 g of ferric chloride ($FeCl_2 \cdot 4H_2O$) in 100 mL of distilled water; simultaneously, a solution of ferric chloride was prepared by adding 6.48 g of ferric chloride ($FeCl_3$ anhydrous) to 100 mL of distilled water. Both solutions were kept separately in a continuous magnetic stirrer at 40 °C. Later, both solutions were mixed, which gave a brown colour. The mixed ferric and ferrous suspension was slowly added dropwise into a suspension of powdered activated bamboo carbon (ABC) under continuous stirring at 40 °C for 1 h. Simultaneously, 2 M NaOH solutions were prepared and added dropwise to the mixed suspension until the pH was 10. The suspension turns into black precipitation from a brown colour.

Further, the suspension was ultrasonicated for 15 min to separate the solid and solution, and it was aged for 24 h. The suspension was washed 6 times with an ethanol–water ratio (1 : 2) and dried overnight in the oven at 60 °C. The final product was appropriately ground, and the obtained nano-magnetite-activated bamboo carbon (MABC) was preserved in desiccator airtight bottles. Fig. 1(c) shows the detailed synthesis process of nano-magnetite-activated bamboo carbon (MABC NPs). The demo of the MABC NPs was separated from the water using a bar magnet, as shown in Fig. 1(c). These exhausted MABC NPs can be reused for further sorption analysis.

2.2 Characterisation techniques

2.2.1 X-ray diffraction (XRD). The XRD patterns of the synthesised powdered BC, ABC, and MABC were obtained using a diffractometer (model Rigaku, D/Max 2200) outfitted with a Cu Kα radiation source at an accelerating voltage of 40 kV (λ = 1.5406 Å; $2\theta = 20$–$80°$; count rate = $2d\ \mathrm{min}^{-1}$). The phases of the synthesised nanosorbents were determined using JCPDS files, and crystal sizes were determined using Scherer's equation:

$$D = \frac{\kappa\lambda}{\beta \cos\theta}, \quad (1)$$

where λ is the wavelength of Cu Kα radiation (1.54 Å), D is the particle size in Å, K is a constant associated with the Miller index of crystallographic planes (given a value of 0.9), β is the full width at half maximum in radians (FWHM), and θ is the Bragg angle.

2.2.2 SEM (scanning electron microscope). A scanning electron microscope (model JSM-IT200 JEOL, Japan) at 20 kV accelerating voltage with an energy-dispersive X-ray micro-analysis system was used to examine the morphology; spot elemental and mapping investigations were performed. Samples were applied to a double-stick carbon tape held in place by an aluminium support stub.

2.2.3 DLS (dynamic light scattering). DLS was used to determine the hydrodynamic radius of the synthesized nanosorbents at a scattering angle of $\theta = 90°$ and laser He/Ne (λ = 632.8 nm) using an LS spectrometer, serial no. LS-0713-0035, Switzerland. A stock-Einstein connection connects the diffusion coefficient to the appropriate, effective hydrodynamic radius:

$$R_h = \frac{k_B}{6\pi\eta D}, \quad (2)$$

where η is the solvent viscosity, T is the absolute temperature and k_B is the Boltzmann constant.

2.2.4 Zeta potential. The zeta potential was used with a zeta analyser to determine the overall charge on the BC, ABC, and MABC surfaces (ZEECOM, Microtec Co., LTD, Japan).

$$Z \approx \varphi = 4\pi\left(\frac{\sigma}{\varepsilon\kappa}\right), \quad (3)$$

where ε and κ are the solution's dielectric constant and the Debye–Huckel parameter, respectively, and σ is the particle's surface charge density. Zeta potential, *i.e.*, the surface potential, can be determined from the potential at the hydrodynamic slip plane. The equation $Z = 4\pi(\mu\eta/\varepsilon)$ describes the link between mobility (m) and zeta potential. In other forms, mobility μ can be written as $\mu = \sigma/\eta\kappa$, where n is the viscosity of the solution.

2.2.5 FTIR (Fourier transform infrared spectroscopy). Synthesised nanosorbents were identified using FTIR in the ATR mode (PerkinElmer, Spectrum 1 US) with wavenumbers ranging from 4000 to 400 cm^{-1}. Samples were made by combining 100 mg of KBr powder as a carrier and 1% of nanocomposite and then pressing the mixture into pellets.

2.2.6 UV-visible absorption. The UV-visible absorption study of BC, ABC, and MABC was performed using a T90+ UV-vis spectrophotometer.

2.2.7 Vibrating sample magnetometer. A Vibrating Sample Magnetometer (VSM) was employed to measure the magnetic saturation of iron oxide. For accurate detection by the VSM analyser, it was necessary for the magnetic moment of the

samples to exceed 10^{-6} emu. A smaller sample size with a vertical orientation was utilised to enhance accuracy, which outperformed the baseline coil detection dimension. It is advisable to position the samples with a 35 mm offset. The coil set's height should be 40 mm, ensuring that the offset aligns with the end of the sample holder. The sample was securely placed within a holder integrated into an Optical Magneto-Mechanical Device (OMMD). Subsequently, the power supply was activated, and the voltage was fine-tuned to 3 V. The magnetisation and hysteresis loops were measured at 25 °C by applying a vibrating sample magnetometer, VSM model no (ADE-EV9).

2.2.8 BET (Brunauer–Emmett–Teller). N_2 adsorption–desorption isotherm investigations were performed at liquid nitrogen (temperature 77 K) through a Quanta Chrome analyser (model Autosorb-1). A sample of 0.15 g MABC NPs was degassed at a temperature of 150 °C for 6 h before adsorption measurements. The surface area, pore diameter, and pore volume were determined using the BET model.

2.3 Toxicity testing of synthesized nanoparticles against prokaryotes

2.3.1 Preparation of broth culture. The *Escherichia coli* strains were picked from the master plate and suspended in Luria Bertani Broth under sterile conditions. The tubes were then incubated for 16–18 h at 37 °C using a shaking incubator until turbidity of 0.5 McFarland units.

2.3.2 Agar disk diffusion method. The LB agar plates were swabbed with the prepared bacterial broth of *E. coli* using a sterile cotton swab. Different concentrations of BC, ABC and MABC NPs were prepared (0.5, 1, 2 and 4 mg mL^{-1}). Using sterile forceps, a sterile disk was first dipped into the nanoparticles, allowed to dry and placed on the agar plate. For a positive test control, a kanamycin disk was placed on the plate along with a negative control containing Milli Q water. The plates were incubated for 24 h at 37 °C and were observed after 24 h for the formation of a zone of inhibition.

2.4 Toxicity testing of nanoparticles against eukaryotes using the spread plate method

Caenorhabditis elegans populations were maintained on nematode growth agarose media (NGMA) (peptone, NaCl, agarose, and agar). The plates were swabbed with an OP50 *E. coli* strain. Along with the bacterial strain, the highest concentration (4 mg mL^{-1}) of BC, ABC and MABC were poured on the media plates. 10 μL of *C. elegans* washed with M9 buffer was transferred on the plates and was then incubated at 20 °C using a BOD incubator for 1 week. The growth pattern and reproductivity of *C. elegans* were observed.

2.5 Adsorption experiments

The fluoride stock solutions were prepared by adding 1 g of sodium fluoride (NaF) in 1000 mL of distilled water. A drop of concentrated nitric acid (HNO_3) was used as an analyte to keep the solution fresh. Adsorption studies for F^- ion removal by MABC NPs were conducted in batch mode. The solution pH effect on F^- ions was examined at various initial pHs: 1 to 8. The pH solution was adjusted using 1 M NaOH and HCl. The effect of contact time and adsorbent dose on F^- ions sorption at various time intervals (10–60 min) and MABC NP dosage (0.01, 0.02, 0.03 and 0.04 g L^{-1}) were performed. The sorption equilibrium studies were conducted at various temperatures, 25, 35, and 45 °C, by dispersing 0.02 g MABC NPs in 50 mL of 4 mg L^{-1} F^- ions (shaking speed = 200 rpm for 1 h). Then, the samples were filtered using a Whatman (no. 42) filter paper, and F^- ions were tested using a fluoride ion selective electrode (AUTO-PF-20-1). The F^- adsorbed on MABC NPs per unit mass was calculated using eqn (4). The adsorption percentage of F^- ions was calculated from eqn (5).

$$q_e = \frac{(C_i - C_e) \times V}{W}, \quad (4)$$

$$S = \frac{(C_i - C_e)}{C_i} \times 100\%, \quad (5)$$

where q_e is the amount of F^- ions adsorbed per gram of MABC NPs (mg g^{-1}). C_i and C_e are the initial and final equilibrium fluoride ions concentration (mg L^{-1}), respectively. V is the volume (L), W is the weight (g) of the adsorbent, and S is the adsorption percentage of fluoride ions.

3. Results and discussion

3.1 XRD analysis

The XRD patterns of carbon materials BC, ABC and MABC are shown in Fig. 2(a–c). For the activated carbon, the diffraction profiles exhibit two broad peaks at approximately 2θ values of 24° and 42°, which are assigned to the reflection from the (002) and (100) planes of the amorphous carbon, respectively. Accordingly, no pronounced graphitisation occurs under the present carbonisation/activation condition. The peak representing (002) slightly sharpens, and the intensity of the peak representing (100) increases after activation with HNO_3.[30,31] This

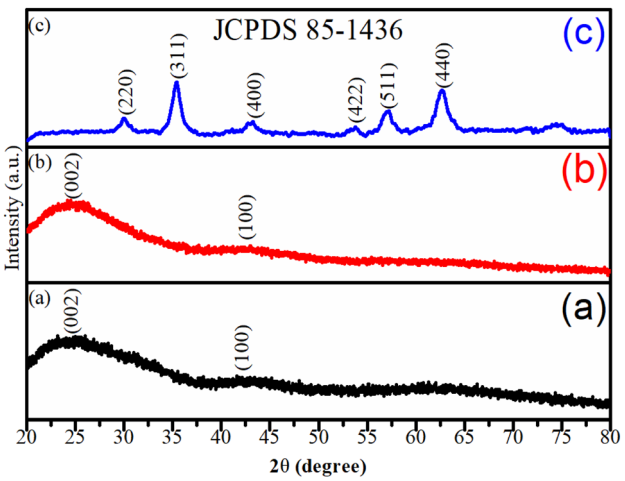

Fig. 2 (a–c) XRD plots of (a) bamboo carbon (BC), (b) activated bamboo carbon (ABC), and (c) magnetite-activated bamboo carbon (MABC) NPs.

result indicates that carbon tends to crystallise although it has a non-graphitized structure.[31]

However, the XRD pattern of MABC [Fig. 2(c)] showed the crystalline nature, with peaks at 2θ values of (29.8°, 35.3°, 43.2°, 53.7°, 57.1°, and 62.6°) corresponding to the Miller planes obtained at (220), (311), (400), (422), (511) and (440), respectively, which are the characteristic peaks of inverse-spinel and face-centred cubic (FCC) structure of Fe_3O_4 NPs matching with JCPDS (card no. 85-1436).[32,33] The result indicated that impregnation with magnetite NPs effectively resulted in crystalline MABC NPs, which was consistent with those reported in the literature.[32–34] The average crystalline size of MABC NPs was obtained from the most intense peak corresponding to the Miller plane (311) using the Debye–Scherer formula (eqn (1)). The estimated crystalline size of the MABC NPs was 8.8 nm.

3.2 Study of morphology and elemental composition

The scanning electron microscope images and EDX spectra illustrate the surface morphologies and element composition of the adsorbents. Fig. 3(a–d) shows the comparative SEM images of bamboo carbon (BC) and activated bamboo carbon (ABC) at different magnifications. The SEM images revealed that carbonised bamboo carbon (BC) pyrolysed at 400 °C maintained the original structural features of bamboo in terms of texture, including bamboo fibres and parenchyma cells [Fig. 3(a and b)]. Further, well-built large, regular, and neatly organized pores, quantifying <5 μm, were detected in the longitudinal section of the BC.[30,31] After the activation of BC with HNO_3 ratio 1 : 2 (2.25 mL HNO_3 : 4.5 mL DI) at 400 °C, large macropores oriented parallel to the fibres were retained, and several nano-sized pores may have been established on the surface of the AC due to breaking of internal bonding. The SEM images of the activated carbon show a partially enlarged view of pores with abundant thick and circular pores, which could be macropores, leading to branching micropores in the interiors of the activated carbon. AC has a tubular and porous structure with a smooth surface, while after being loaded with magnetite NPs on the surface of activated carbon, the nanoparticles are agglomerated and stuck to each other on the surface of activated carbon, thus making the surface rough and coarse [Fig. 4(a and b)].

Fig. 5(a–c) shows the SEM-EDX analysis of BC, ABC and MABC NPs. BC shows the presence of carbon (67.33%) and oxygen (32.67%). EDX analysis of ABC shows the presence of carbon (68.42%) and oxygen (31.58%) [Fig. 5(b)]. MABC NPs indicate the presence of carbon (3.43%), iron (75.01%) and oxygen (21.56%), as shown in Fig. 5(c). The results confirm that no impurities are present in the formation of activated carbon. The presence of iron shows the successful grafting of magnetite NPs onto ABC.

3.3 UV absorbance analysis

The UV-visible absorption spectra of the synthesised BC, ABC, and MABC NPs are presented in Fig. 6(a–c), which shows a prominent peak at 271 nm, indicating the formation of BC,

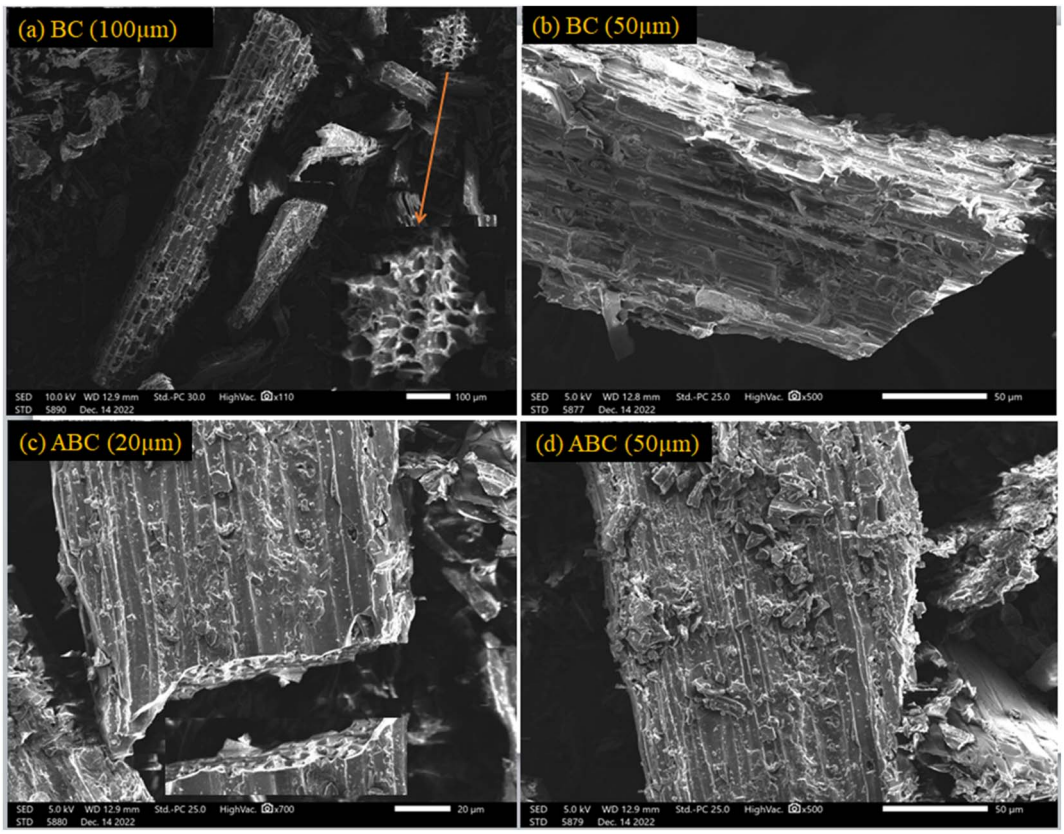

Fig. 3 (a–d) SEM images of (a and b) bamboo carbon (BC) at 50 and 100 μm; (c and d) ABC at 20 and 50 μm.

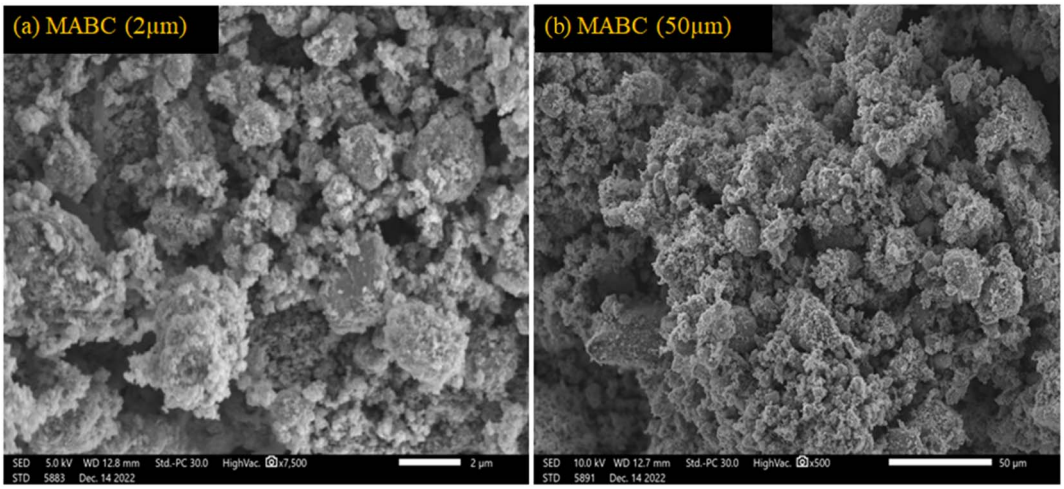

Fig. 4 (a and b) SEM images of MABC at 2 μm and 50 μm.

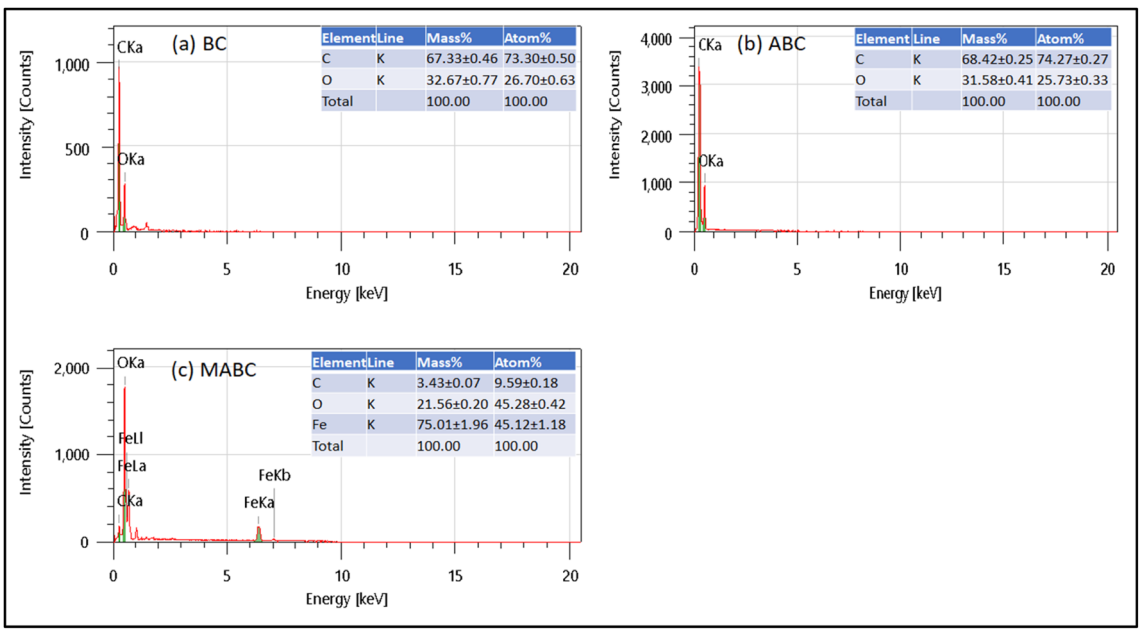

Fig. 5 (a–c) SEM/EDX spectra of (a) BC, (b) ABC, and (c) MABC NPs.

ABC, and MABC. This was attributed to the π–π* transition of the aromatic sp^2 carbon.[35–38] Although IR spectral analysis confirms the presence of the C–O group, no absorption peaks corresponding to the n–π* transition are observed.[39,40] Additionally, one peak was observed at 384 nm because of the M–O band as a result of the stretching vibration of the Fe–O bond in Fe_3O_4 NPs [Fig. 6(c)].

3.4 Zeta potential and hydrodynamic size measurements

Fig. 7(a–c) shows the surface charge potential of BC, ABC, and MABC NPs obtained using the zeta potential technique. The adsorbents BC, ABC and MABC NPs were dissolved in 20 mL of DI water. Zeta potential measurements give a highly positive surface charge of 70.19 mV for BC, 65.90 mV for ABC and 71.83 mV for MABC NPs. The positive surface charge could be due to an upsurge in hydrogen ion (H^+) concentration through dissociation.

The zeta potential is a vital function of pH; the point where the zeta potential is zero is called the point zero charge pH (pH_{PZC}). The zeta potential analysis was performed at various pH solutions (1–10) to obtain the point zero charge pH (pH_{PZC}) of MABC NPs. The pH_{PZC} of MABC was obtained in an acidic solution with pH 1, as shown in Fig. 7(d). The zeta potential of MABC was positive in acidic pH 2–6, and beyond that, it acquired a negative zeta potential. The positive zeta potential in acidic pH is due to the upsurge in hydrogen ion (H^+) concentration through dissociation. Conversely, MABC attained negative zeta potential at alkaline solution pH due to the increased hydroxide (OH^-) ion concentration.

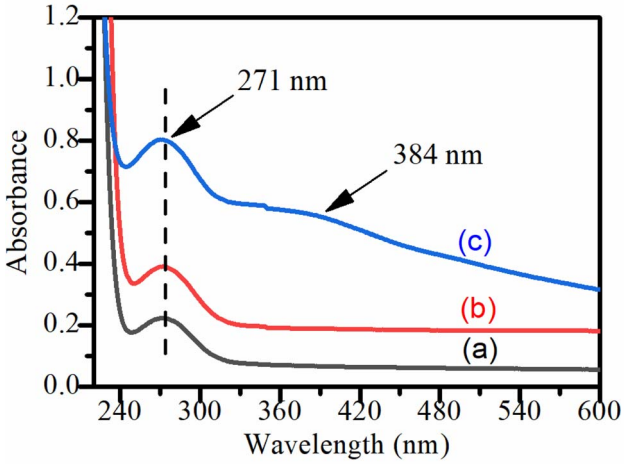

Fig. 6 (a–c) UV-vis absorbance plots of (a) bamboo carbon (BC), (b) activated bamboo carbon (ABC), and (c) magnetite-activated bamboo carbon (MABC).

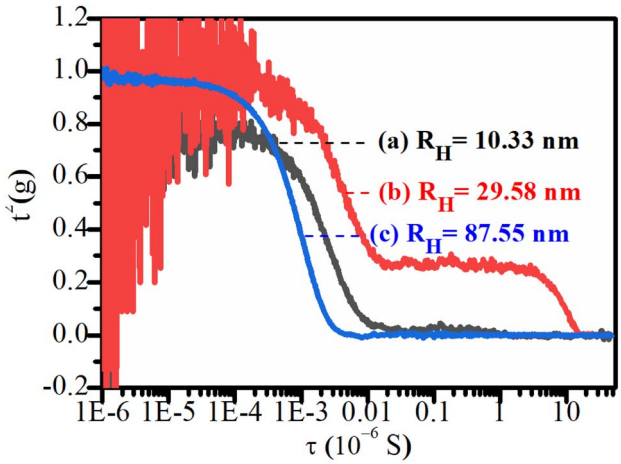

Fig. 8 (a–c) DLS of (a) bamboo carbon (BC), (b) activated bamboo carbon (ABC), and (c) magnetite-activated bamboo carbon (MABC).

Fig. 8(a–c) shows the DLS plot of (a) BC, (b) ABC and (c) MABC NPs. The hydrodynamic size of the adsorbent dispersed in distilled water, which was larger than the actual size, was determined by DLS. The hydrodynamic diameters obtained for BC, ABC, and MABC were 10.33 nm, 29.58 nm, and 87.55 nm, respectively.

3.5 Fourier transform-infrared spectroscopy study

Fig. 9(a–c) shows the FTIR spectra corresponding to BC, ABC, and MABC recorded in a 4000–400 cm^{-1} wave number range, respectively. The band that appeared at 3360 cm^{-1} in the curve (a–c) is due to the stretching vibrations of the –OH group.[41] The spectra exhibited adsorption peaks at 2992 cm^{-1} and 2898 cm^{-1}, which were attributed to the symmetric stretching of C–H and O–H bending and C–H stretching, respectively.[42] The

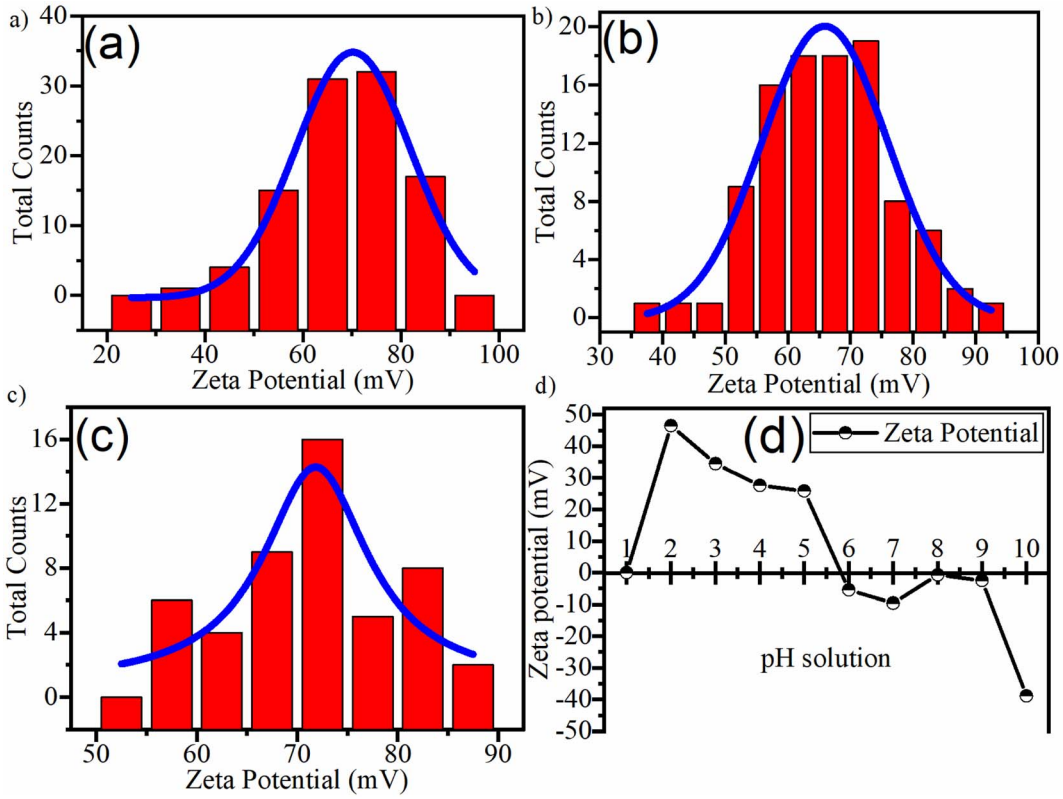

Fig. 7 (a–d) Zeta potential of (a) bamboo carbon (BC), (b) activated bamboo carbon (ABC), (c) magnetite-activated bamboo carbon (MABC), and (d) point zero charge plot of MABC with solution pH (1–10).

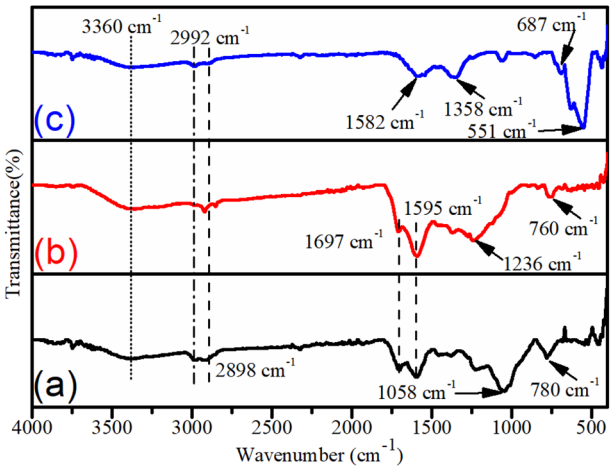

Fig. 9 (a–c) FTIR spectra of (a) bamboo carbon (BC), (b) activated bamboo carbon (ABC), and (c) magnetite-activated bamboo carbon (MABC).

bands appearing at 1697 cm^{-1}, 1595 cm^{-1}, 1236 cm^{-1}, and 760 cm^{-1} were attributed to C=C stretching, C=O stretching, C–O stretching, and C–H out-of-plane deformation, respectively. These functional groups represent the formation of BC. Fig. 9(b) shows the characteristic peak at 3360 cm^{-1} attributed to O–H stretching.[42] The spectra exhibited adsorption peaks at 2992 cm^{-1} and 2898 cm^{-1}, which were attributed to symmetric stretching of C–H and O–H bending and C–H stretching, respectively. The peaks appearing at 1697 cm^{-1}, 1595 cm^{-1}, 1058 cm^{-1}, and 780 cm^{-1} were attributed to C=C stretching, C=O stretching, C–O stretching, and C–H out-of-plane deformation, respectively.[43] The surface of the prepared activated bamboo carbon has these functional groups that confirm the formation of ABC. The FT-IR spectra of the MABC were obtained to characterize the structure of the carbon phase and iron oxides. In Fig. 9(c), the peak at 3360 cm^{-1} depicts OH stretching. The peaks at the 2992 cm^{-1} and 2898 cm^{-1} spectra represent the symmetric stretching of C–H and O–H bending and C–H stretching, respectively. The 1582 cm^{-1} and 1358 cm^{-1} peaks show the characteristic peaks of the aromatic ring's C=O stretching and C=C vibration, respectively. The peak occurring at 687 cm^{-1} indicates the CH out-of-plane deformation structures in the obtained MABC. In addition, there are Fe_3O_4 NPs in the intense peak at 551 cm^{-1} due to the M–O band, which is assigned to the stretching vibration of the Fe–O bond in magnetite NPs.[8,35] The detailed information of spectral data of BC, ABC and MABC are listed in Table 1.

3.6 BET surface area analysis

The comparative BET surface area and porosity of the ABC and MABC NPs were assessed using nitrogen physisorption measurements. The BET curve, a typical type IV isotherm, is shown in Fig. 10. The obtained BET surface areas of MABC and ABC were 73.45 $m^2\ g^{-1}$ and 10.03 $m^2\ g^{-1}$, respectively. The average pore diameter, pore volume and total pore volume of MABC were obtained as 60.89–56.98 Å, 0.087–0.096 $cm^3\ g^{-1}$ and 0.094 $cm^3\ g^{-1}$, respectively. Moreover, for ABC, the average pore radius, pore volume and total pore volume were obtained as 19.153–17.035 Å, 0.012–0.010 $cm^3\ g^{-1}$ and 0.949 $cm^3\ g^{-1}$, respectively. It is clear from comparative Table 2 that the BET surface area, pore volume, and pore size of ABC increased after being grafted with magnetite NPs. This is because some pores of ABC are partly enclosed after being assorted with magnetite NPs, thereby increasing the pore size, pore volume, and BET surface area.

This substantial increase in the surface area (pore size) of MABC was advantageous for various applications, including its use as a sensing or energy storage material and water

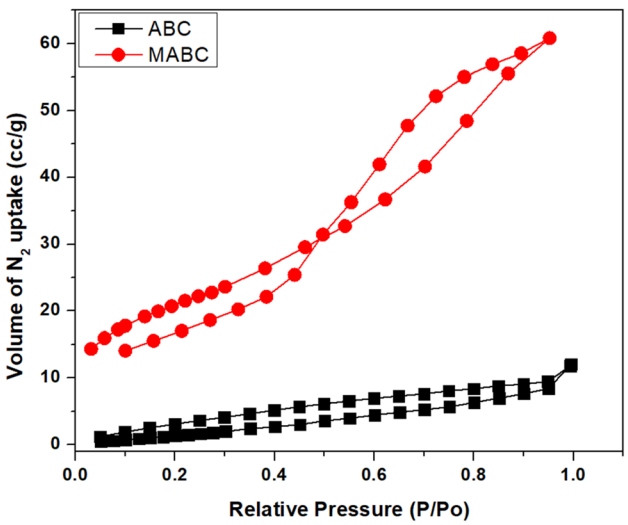

Fig. 10 BET plot of ABC and MABC NPs.

Table 1 Detailed information spectral data of BC, ABC and MABC

BC		ABC		MABC	
3360 cm^{-1}	OH stretching	3360 cm^{-1}	OH stretching	3360 cm^{-1}	OH stretching
2992 cm^{-1}	Symmetric stretching of C–H	2992 cm^{-1}	Symmetric stretching of C–H	2992 cm^{-1}	Symmetric stretching of C–H
2898 cm^{-1}	O–H bending, C–H stretching	2898 cm^{-1}	O–H bending, C–H stretching	2898 cm^{-1}	O–H bending, C–H stretching
1697 cm^{-1}	C=C stretching	1697 cm^{-1}	C=C stretching	1582 cm^{-1}	C=O stretching
1595 cm^{-1}	C=O stretching	1595 cm^{-1}	C=O stretching	1358 cm^{-1}	C=C vibration of the aromatic ring
1058 cm^{-1}	C–O stretching	1236 cm^{-1}	C–O stretching	687 cm^{-1}	CH out of plane deformation
780 cm^{-1}	CH out of plane deformation	760 cm^{-1}	CH out of plane deformation	551 cm^{-1}	Stretching vibration of Fe–O bond in magnetite

Table 2 Surface texture information of MABC NPs and ABC obtained from N_2 adsorption–desorption plots

Nanomaterial	BET surface area ($m^2\ g^{-1}$)	Pore volume ($cm^3\ g^{-1}$)	Pore size (Å)
MABC NPs	S_{BET} = 73.44	BJH adsorption: pore volume = 0.087	BJH adsorption: pore diameter (d) = 60.89
	BJH adsorption: surface area = 57.45	BJH desorption: pore volume = 0.096	BJH desorption: pore diameter (d) = 56.98
	BJH desorption: surface area = 67.93	Total pore volume = 0.094	
ABC NPs	S_{BET} = 10.030	BJH adsorption: pore volume = 0.012	BJH adsorption: pore radius = 19.153
	BJH adsorption: surface area = 8.079	BJH desorption: pore volume = 0.010	BJH desorption: pore radius = 17.035
	BJH desorption: surface area = 7.089	Total pore volume = 0.949	

purification.[36,37] The comparative surface texture information of ABC and MABC NPs obtained from N_2 adsorption–desorption plots are listed in Table 2.

3.7 Vibrating sample magnetometer study

The magnetic field and magnetic strength of the MABC NPs were assessed using a vibrating sample magnetometer (VSM) technique. In the magnetisation process, as depicted in Fig. 11, the VSM magnetic hysteresis curves for MABC NPs show superparamagnetic behaviour due to magnetite NPs grafted into activated bamboo carbon.[36] This phenomenon is typically observed in magnetic materials when an external magnetic force is applied, causing the particles within the material to exhibit magnetism.[37] The magnetic hysteresis loop represents the saturation magnetisation of MABC NPs measured at 22.46 emu g^{-1}, revealing the saturation magnetisation attributed to the presence of magnetite NPs. Furthermore, this result indicates the presence of robust magnetic properties in magnetite-activated bamboo carbon (MABC). Grafting magnetite NPs into activated bamboo carbon improves the specific adsorption capacity and easily separates MABC NPs from the aqueous media using a bar magnet. This can solve the leaching problems of nanosorbents in water and can be reused for further sorption analysis, as shown in Fig. 1(d).

3.8 Surface wettability (contact angle)

The attractive and repellent strength force is related to the "contact angle" between the surface and the water drop. In a hydrophilic surface, the contact angle is <90°; hence, the water drop tends to spread out and wet the surface. In a hydrophobic surface, the contact angle is >90°, and the water drop tends to bead up on the surface. The liquid drop is pulled towards the surface and spread along the surface when the adhesive forces are attractive (the liquid is attracted to the solid surface). The surface is called "hydrophilic", and it is called water-loving. If the adhesive forces are repellent (the solid surface repels the liquid), the liquid drop minimises its contact with the surface, and the surface becomes "hydrophobic".

Fig. 12(a–c) shows the images of the water contact angle (CA) measured in a static state for (a) BC, (b) ABC, and (c) MABC droplets. The syringe placed a water drop on each surface of the sample, and the contact angle was quantified at the interface of the surface. The contact angle of BC was measured at 46.3°, indicating that it was slightly hydrophilic [Fig. 12(a)]. After the activation (acid treatment) of BC, the contact angle was estimated at 26.7° [Fig. 12(b)], showing a highly hydrophilic nature compared to BC due to the functional group. The CA of MABC was obtained to be 61.8°, showing less hydrophilic behaviour with a drastic change [Fig. 12(c)] compared to BC and ABC. During the synthesis process, the surface of ABC was transformed from hydrophobic to highly hydrophilic. This demonstrates that ABC is a less hydrophobic material attributed to a few –OH groups on the surface of ABC. In conclusion, ABC has high surface roughness and lowers the surface energy; a large amount of air is trapped in the interspaces or cavities that convert ABC from hydrophobic to hydrophilic compared to BC and MABC.

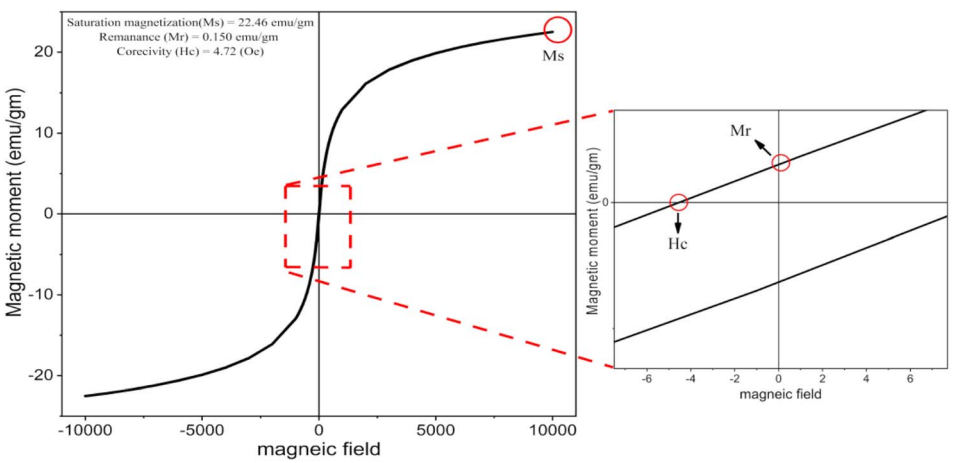

Fig. 11 Vibrating sample magnetometer (VSM) plot of MABC NPs.

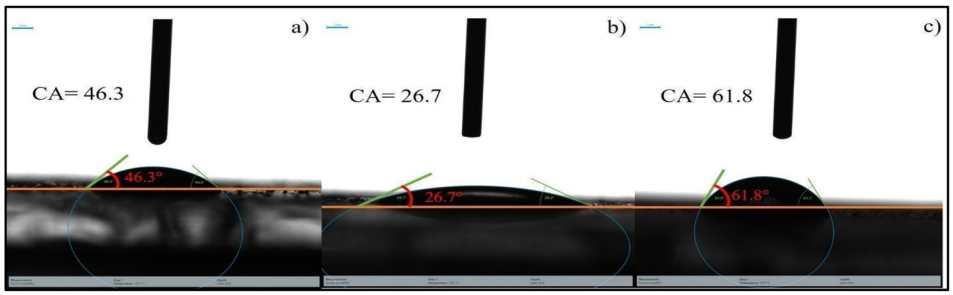

Fig. 12 (a–c) Contact angle measurements of (a) bamboo carbon (BC), (b) activated bamboo carbon (ABC), and (c) magnetite-activated bamboo carbon (MABC).

3.9 Antimicrobial testing of BC, ABC, and MABC NPs

The antimicrobial properties of BC, ABC and MABC NPs at different concentrations (0.5, 1, 2 and 4 mg mL^{-1}) were performed against prokaryotes (*E. coli* – OP50) in the LB agar plates swabbed with bacterial culture. The synthesized nanosorbents showed no antimicrobial properties, even at high doses (4 mg mL^{-1}). However, the kanamycin disk showed a zone of inhibition of 23 mm, 20 mm and 21 mm as shown in Fig. S1(a–h) (ESI File).† Thus, the result indicates the nontoxic nature of BC, ABC and MABC NPs.

3.10 Cytotoxicity testing of BC, ABC, and MABC

The cytotoxicity test of prepared nanosorbents BC, ABC, and MABC was performed using a plate containing a 4 mg mL^{-1} concentration of NPs spread along with *E. coli* (OP50 strain). No discrepancy in the growth and reproduction of *C. elegans* was observed when compared with the control plate, as shown in Fig. S2(a–h) (ESI File).† 4 mg mL^{-1} concentration of BC, ABC and MABC NPs spread along with *E. coli* (OP50 strain) did not harm the growth and reproduction of nematodes. After 1 week of incubation, it was observed that different stages of nematodes (L1–L4) grow and reproduce (lay eggs). The result indicates that the synthesized nanosorbents BC, ABC and MABC NPs are highly non-toxic and eco-friendly, thereby indicating highly biocompatible nanosorbents. The result shows the nontoxic nature of BC, ABC and MABC NPs, thereby holding significant promise for addressing water quality challenges using sustainable, eco-friendly nanosorbents.

4. Adsorption studies of fluoride ions

Comparative fluoride ion removal studies were analysed using ABC and MABC NPs. The sorption studies were performed using 20 mg L^{-1} NP doses dissolved in F^- concentration (4 mg L^{-1}) in 40 mL solution at optimal parameters (pH: 5; temp.: 25 °C; shaking speed: 200 rpm; agitation reaction time: 60 min). It is clear from Fig. 13 that both ABC and MABC successfully adsorbed F^- ions from water. The removal efficiency of fluoride ions using the adsorbent MABC is extremely higher compared with ABC. About 99.6% of F^- ions were adsorbed using MABC, and 75.9% were adsorbed using ABC. The excellent adsorption of F^- ions using MABC NPs is due to the grafting of magnetite

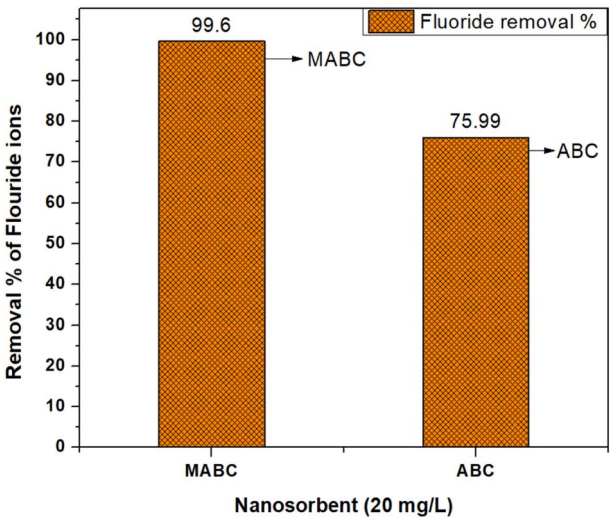

Fig. 13 Comparative fluoride adsorption using MABC and ABC.

NPs onto activated bamboo carbon. The excellent properties of magnetite nanoparticles, such as high surface area, biocompatible, superparamagnetic, and hydrophilic nature, enhanced the removal efficiency of fluoride ions. Furthermore, magnetite NPs grafted onto activated bamboo carbon enhanced the magnetic properties of activated bamboo carbon, thereby easily stripping out MABC NPs from fluoride-contaminated water and reusing them for further sorption analysis. Thus, MABC NPs were used as sorbents for the rest of the fluoride ion adsorption parameters.

4.1 Effect of the MABC dose

Fig. 14(a) shows the effect of the adsorbent MABC dose on aqueous fluoride ion removal. The fluoride ion sorption experiment was conducted in an initial F^- concentration (4 mg L^{-1}) in 50 mL solution by varying the MABC NP dosage (0.01, 0.02, 0.03 and 0.04 g L^{-1}) under optimum experimental conditions (pH 5, temp: 25 °C, shaking: 200 rpm, agitation reaction time: 60 min). It is clear from the plots that increasing the MABC dose increases the removal percentage (R%) of fluoride ions. The F^- ion removal efficiency increased substantially from 38 to 99% with increases in adsorbent dosage (0.01–0.02 g L^{-1}), thereby indicating an increase in adsorbent dosage while increasing the

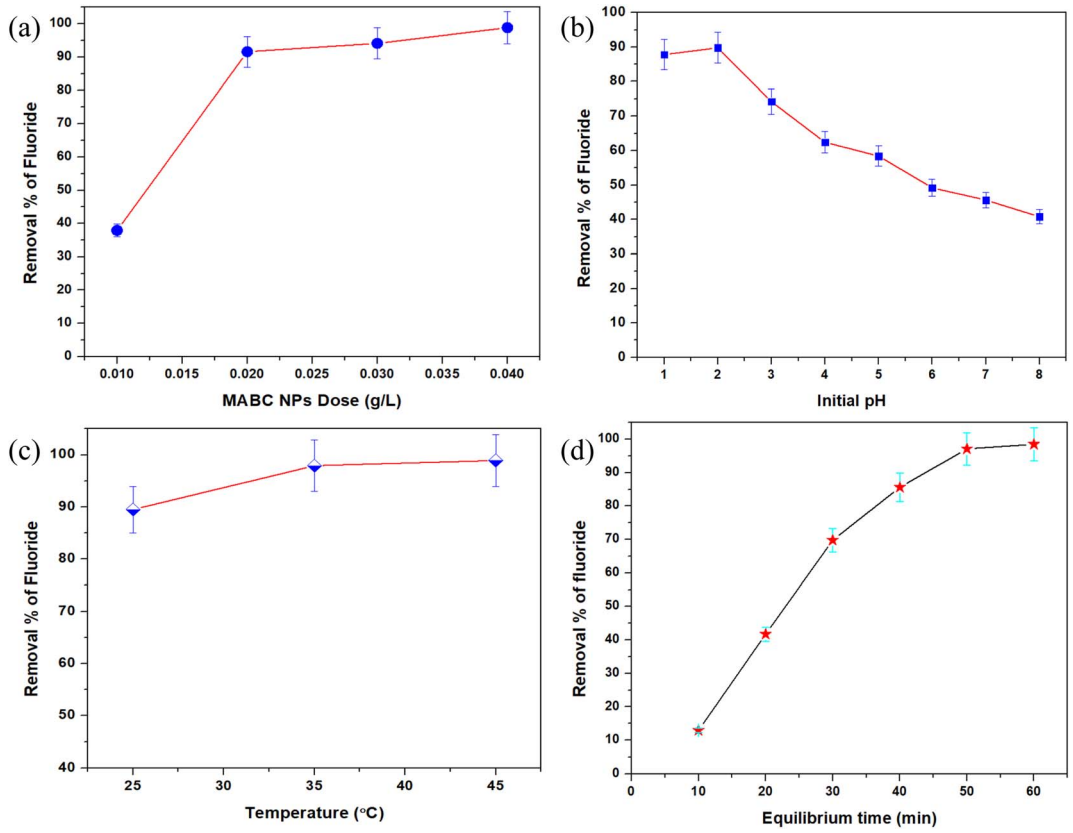

Fig. 14 (a) Effect of MABC NP dose (0.01–0.04 g L^{-1}) on removing fluoride ions. (b) Effect of aqueous pH (1–8) on fluoride ion adsorption. (c) Effect of temperature (25, 35, and 45 °C) on the removal of fluoride ions. (d) Effect of agitation times (10, 20, 30, 40, 50, 60 min) on fluoride ion removal.

number of active sites of adsorbents for binding F^- ions.[8] The equilibrium region of the removal efficiency of F^- ions reached 0.02 g L^{-1} of dosage; after that, there was no further binding. Thus, a 0.02 g L^{-1} of MABC NP dose was fixed in all the adsorption studies.

4.2 Effect of initial pH

The effect of the solution pH on the DE-fluoridation process is one of the essential parameters that relates to the active surface sites (protonated or deprotonated) of the adsorbent material and the adsorbate's degree of ionization in the solution.[38] Fig. 14(b) displays the effect of solution pH (1.0–8.0) on the removal percentage of fluoride ions by MABC. The experiment was carried out under optimal conditions (temp: 25 °C, shaking: 200 rpm, reaction time: 60 min) by adding 0.02 g L^{-1} of MABC NPs in 50 mL solutions containing 4 mg L^{-1} of F^- ions adjusted at different pH from 1.0 to 8.0. As shown in Fig. 14(b), the fluoride removal efficiency of MABC increased significantly at acidic pH 1.0–2.0. However, it decreased as the pH increased from 3.0 to 8.0. The maximum fluoride removal efficacy was 89.0–90.5% at acidic pH (1.0–2.0). Moreover, a decrease in fluoride removal was observed under highly alkaline (pH ~8.0) conditions. From the experimental data, the pH_{ZPC} values for MABC were at pH 1.0 [Fig. 7(d)]. The behaviour of fluoride ion adsorption onto MABC can be analysed by considering the adsorbent's point of zero charges (pH_{ZPC}). When the pH is lower than pH_{ZPC}, the adsorbent surface is positively charged; when it is higher than pH_{ZPC}, the adsorbent surface is negatively charged. Thus, the defluoridation efficiency is reduced for MABC when pH > pH_{ZPC} due to electrostatic repulsion between fluoride ions and negatively charged adsorbent surface and competition between fluoride ions and excess hydroxyl anions. However, the high removal efficiency of fluoride ions at pH < pH_{ZPC} is due to electrostatic attraction.[8] Hence, the maximum removal of fluoride ions is obtained in acidic pH 1–2. Similar pH profiles have been reported in fluoride adsorption onto tea waste supported by hydrous aluminium oxide nanoparticles.[38] The binding mechanism of fluoride ions with MABC NPs is shown in Scheme 1.

4.3 Effect of temperature

To analyse the effect of temperature on fluoride ion adsorption onto MABC NPs, the experiment was conducted under certain experimental conditions (aqueous pH 5, 200 rpm, and agitation time: 60 min) by adding 0.02 g per L MABC NPs in an initial concentration of 4 mg F^- per L at varying temperature (25, 35, and 45 °C). It is clear from Fig. 14(c) that the removal of F^- ions increased with an increase in temperature, which is an endothermic process in nature. The increase in F^- ion adsorption with the temperature increase is probably due to a combination

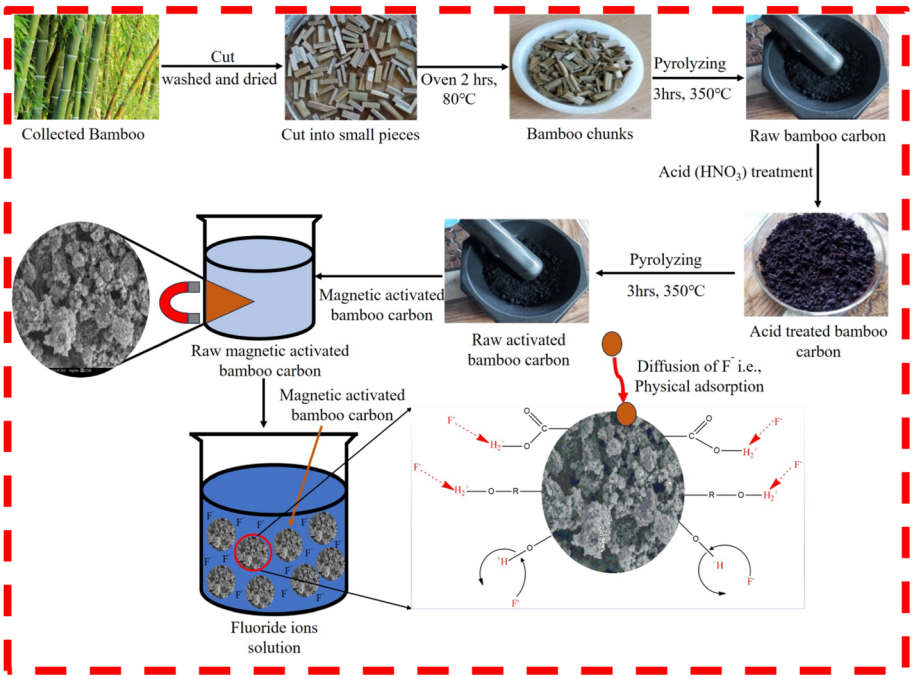

Scheme 1 Diagrammatic representation of the formation of MABC from waste bamboo biomass for the effective remediation of fluoride (F^-) ions from water.

of diffusion and growth in the surface area of the adsorbent caused by oxidation.[44] Such adsorption would widen and deepen the tiny microspores that cause "broadening and expanding of pores", thereby creating more surfaces for adsorption.[45] Thus, the increase in the number of adsorption sites is because of the fractures of internal bonds of particle edge, thereby increasing the removal efficiency of F^- ions from the aqueous solution.[44,45]

4.4 Kinetic studies of F^- ion adsorption (effect of agitation time)

To determine the effect of contact time on the adsorption of fluoride ions on MABC NPs, the experiment was carried out under optimal conditions (solution pH 5, temp: 25 °C, and shaking: 200 rpm). 0.02 g L^{-1} of MABC NPs was added at an initial fluoride concentration of 4 mg L^{-1} in a 50 mL solution at various agitation times (10, 20, 30, 40, 50, and 60 min). It is shown in Fig. 14(d) that fluoride ion adsorption efficiency increased from 12 to 99% with an increase in agitation time from 10 to 60 min. About 12% of F^- ions uptake occurred within 10 minutes and almost 99% within 50–60 minutes. The removal rate was initially rapid and decreased as the equilibrium approached. The adsorption equilibrium was achieved within 50 min of shaking; beyond this, there was no further increase in adsorption. A similar equilibrium time was reported for fluoride adsorption onto carbon nanotubes.[8]

To determine the mechanisms of F^- ion adsorption onto MABC NPs, pseudo first-order and pseudo second order kinetic models were applied. Fig. 15(a and b) shows the variation in the

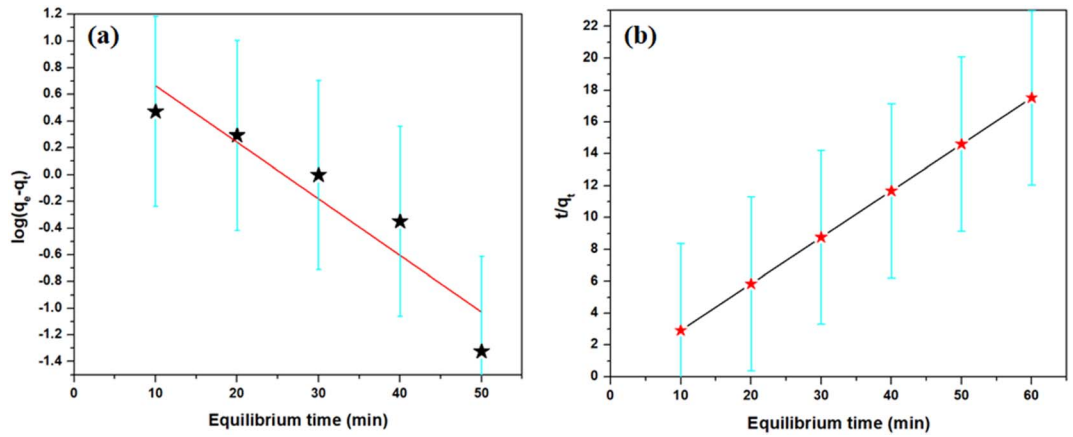

Fig. 15 (a and b) (a) Pseudo-first-order and (b) pseudo-second-order kinetic plot on adsorption of fluoride ions onto MABC NPs.

Table 3 Kinetic model pseudo 1st and 2nd order parameters of fluoride ion adsorption on MABC NPs

Parameters	Pseudo first-order	Pseudo-second-order
Slope (m)	−0.042	0.292
K	0.248	0.292
Intercept (c)	1.0900	1.982
q_e (mg g^{-1})	12.30	95.96
R^2	0.851	1

amount of adsorbed (q_t) as a function of time. The slopes and intercepts, as calculated from the plots, were used to determine the coefficient of determination (R^2) and kinetic rate constant (k) [eqn (6) and (7)]. The fluoride ion adsorption onto MABC NPs for pseudo first and second order kinetic models was 12.30 and 95.96 mg g^{-1}, respectively. The obtained kinetic parameters, *i.e.*, the coefficient of determination (R^2) and kinetic rate constant (k) are illustrated in Table 3.

It is clear from Table 3 that the highest coefficient of correlation determination ($R^2 = 1$) belongs to the pseudo-second-order kinetic model, which provides the best fit with the experimental data of F^- ion removal compared with the pseudo-first-order models ($R^2 = 0.851$), thereby indicating that the adsorption of F^- ions onto the MABC NPs is controlled by chemisorption. Thus, the rate depends on the number of MABC surface sites. In the linear form of these two models, the equations can be written as follows:

Pseudo-first-order kinetic model:

$$\log\log(q_e - q_t) = \log\log(q_e) - \frac{k_1 t}{2.303}. \quad (6)$$

Pseudo-second-order kinetic model:

$$\frac{t}{q_t} = \frac{1}{k_2 q_e^2} + \frac{t}{q_e} \quad (7)$$

Product $k_2 q_e^2$ is the initial sorption rate, represented as rate = $k_2 q_e^2$. Here, k_1 and k_2 (min^{-1}) are the first-order and second-order adsorption rate constants, respectively; q_e is the amount adsorbed at equilibrium; and q_t is the amount of lead absorbed at time 't'.

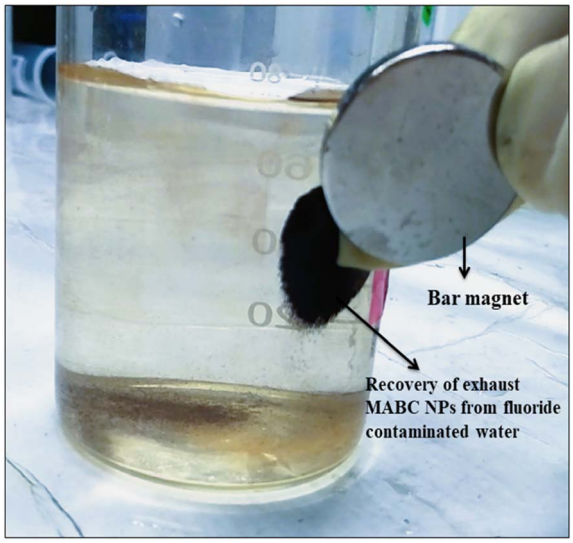

Fig. 16 Exhausted magnetite-activated bamboo carbon (MABC) NPs recovered from fluoride ion-contaminated water using a bar magnet.

The comparative aqueous fluoride ion removal capacity of MABC NPs with other nanosorbents obtained from agricultural-based wastes are listed in Table 4.[46–57] The adsorption capacity of the MABC NPs is greater than the other listed similar adsorbents. Using a bar magnet, MABC NPs can recover quickly from fluoride-contaminated water (Fig. 16), which reduces the water's adsorbent leaching problems, thereby replacing the costly commercial adsorbents.

5. Regeneration studies

The adsorption of fluoride ions on MABC NPs is highly pH dependent; hence, desorption of F^- ions is possible by controlling the aqueous pH. Regeneration studies of exhausted

Table 4 Comparative aqueous fluoride ion removal capacity of MABC NPs with other agricultural-based waste nanosorbents

Sl no.	Type of adsorbent	Metal ions	Removal of fluoride ions (%)	Reference
1	Rice husk	F^-	—	46
2	Cashew nut sheath	F^-	87.60	47
3	Powdered corn cob	F^-	—	48
4	Zirconium-impregnated coconut shell carbon	F^-	90.00	49
5	Zirconium-impregnated cashew nut shell carbon	F^-	80.33	50
6	Zirconium-impregnated groundnut shell carbon	F^-	84.00	51
7	Banana peel	F^-	93.34	52
8	Groundnut shell	F^-	89.90	52
9	Sweat lemon peel	F^-	59.55	52
10	*Citrus Limetta* (mosambi) peel powder	F^-	82.50	53
11	Zirconium(IV) loaded carboxylated orange peel (ZCOP)	F^-	97.20	54
12	*Phyllanthus emblica* (Indian gooseberry)	F^-	82.10	55
13	*Tinospora cordifolia* plant powder	F^-	70.00	56
14	*Ficus religiosa* (peepal) leaves powder	F^-	74.00	57
15	MABC NPs	F^-	99.00	Present work

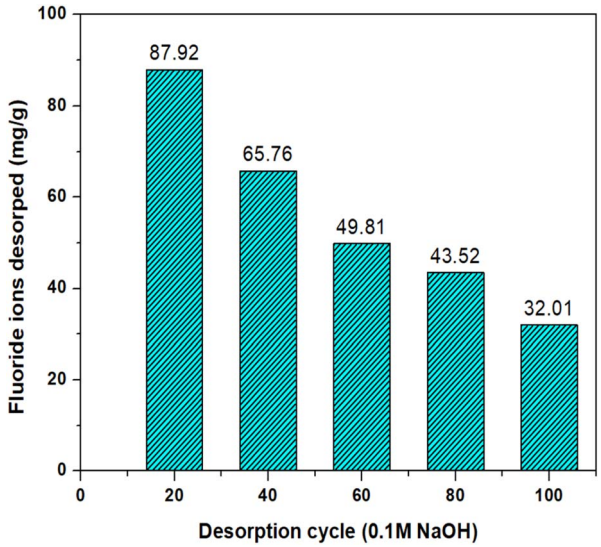

Fig. 17 Regeneration of spent fluoride ion uptake on MABC NPs using 0.1 M NaOH as a desorption agent.

MABC NPs were performed by conducting 5-desorption cycles using 0.1 M NaOH as the desorbing agent. First, 0.02 g L^{-1} of MABC NPs was added to 50 mL of 4 mg L^{-1} F^- ions and placed in a shaker for 1 h at 200 rpm for agitation. The exhausted MABC NPs were recovered from F^- ion contaminated water *via* a bar magnet, as shown in Fig. 16. The recovered exhausted MABC NPs were regenerated by conducting a 5-cycle desorption analysis using 20 mL of NaOH (0.1 M) in each cycle. Fluoride ion desorption from the first to the fifth cycle was 87.9, 65.7, 49.8, 43.8, and 32.01 mg g^{-1}, respectively, as shown in Fig. 17. In the first cycle of 20 mL of NaOH (0.1 M) elutes, 87.92% fluoride ions and the rest were desorbed in the remaining four cycles; after that, no further desorption occurred. Thus, MABC NPs can be regenerated and reused further to remove fluoride ions.

6. Conclusion

Magnetic-activated bamboo carbon (MABC) was successfully derived from waste bamboo chunks grafted with magnetite NPs using the co-precipitation method to obtain stable, cost-effective, nontoxic, and intelligent magnetic nanosorbents for effective fluoride ion removal from water. Structural and morphology studies, BET surface area and porosity, surface charge, and adsorption performance for fluoride ions were systematically investigated. SEM images showed that several pores were disturbed on the bamboo carbon and activated the bamboo carbon's surface, indicating that physical adsorption played a substantial role in fluoride ion sorption. The cytotoxicity and antimicrobial activity analyses of BC, ABC, and MABC were highly nontoxic to both prokaryotes and eukaryotes. These results show that derived nanosorbents are promising for addressing water quality challenges and promoting environmental sustainability in water research and treatment applications. About 99% of F^- ions were removed using a 0.02 g L^{-1} dose of MABC NPs within 50 min. The maximum removal of fluoride ions was obtained at solution pH 2. Increasing the temperature increased F^- ion removal, and the optimal temperature was obtained at 35 °C. The exhausted MABC was recovered from the aqueous solution using a bar magnet. Regeneration studies of exhausted MABC were successfully performed using NaOH (0.1 M) as a desorbing agent. Thus, these studies suggest that bamboo waste-based magnetite-activated bamboo carbon can introduce a new approach to developing a highly stable, biocompatible, and rapid device from biowaste for potentially treating F^- ion contaminated water.

Data availability

The author confirms that the data supporting the findings of this study (Manuscript ID: RA-ART-05-2024-003752) are available within the article and its ESI File.† Raw data that supports the findings of this research article are available from the corresponding author upon reasonable request.

Conflicts of interest

There are no conflicts to declare.

Acknowledgements

This research work was supported by R&D sanctioned project no. PHED/JJM/158/2021-22/483 funded by Jal Jeevan Mission (JJM), Itanagar, under the head account "Water Quality Monitoring & Surveillance" and sub-component "Any Other Innovation". The authors thank the USIC, University of Delhi and AIRF, JNU, New Delhi, for providing BET, SEM, and FT-IR characterization facilities.

References

1 S. Madhav, A. Ahamad, A. K. Singh, J. Kushawaha, J. S. Chauhan, S. Sharma and P. Singh, Water pollutants: sources and impact on the environment and human health, *Sensors in Water Pollutants Monitoring: Role of Material*, 2020, pp. 43–62.
2 M. S. Sankhla, M. Kumari, M. Nandan, R. Kumar and P. Agrawal, Heavy metals contamination in water and their hazardous effect on human health-a review, *Int. J. Curr. Microbiol. Appl. Sci.*, 2016, **5**, 759–766.
3 C. Christophoridis, I. Pasias, E. Mitsika, S. Veloutsou and K. Fytianos, Fluorides in different types of aquatic systems and their correlation with metals and metalloids, *Heavy Metal in Water*, 2014, pp. 261–280.
4 A. V. Aguilar, Extent and Impact of Arsenic and Fluoride Leaching from Hydrothermally Impacted Sediments of the Independence Basin Aquifer System, Doctoral dissertation, The University of Texas at San Antonio, Mexico, 2022.
5 F. Edition, Guidelines for drinking-water quality, *WHO Chron.*, 2011, **38**, 104–108.

6 S. Srivastava and S. J. S. Flora, Fluoride in drinking water and skeletal fluorosis: a review of the global impact, *Curr. Environ. Health Rep.*, 2020, **7**, 140–146.
7 E. Shaji, K. V. Sarath, M. Santosh, P. K. Krishnaprasad, B. K. Arya and M. S. Babu, Fluoride contamination in groundwater: A global review of the status, processes, challenges, and remedial measures, *Geosci. Front.*, 2024, **15**(2), 101734.
8 D. Mohan, S. Kumar and A. Srivastava, Fluoride removal from groundwater using magnetic and nonmagnetic corn stover biochars, *Ecol. Eng.*, 2014, **73**, 798–808.
9 D. Saha and R. K. Ray, Groundwater resources of India: potential, challenges and management, *Groundwater Development and Management: Issues and Challenges in South Asia*, 2019, pp. 19–42.
10 A. Bhatnagar, E. Kumar and M. Sillanpää, Fluoride removal from water by adsorption—a review, *Chem. Eng. J.*, 2011, **171**, 811–840.
11 M. M. Sabzehmeidani, S. Mahnaee, M. Ghaedi, H. Heidari and V. A. Roy, Carbon based materials: A review of adsorbents for inorganic and organic compounds, *Mater. Adv.*, 2021, **2**, 598–627.
12 Y. Wei, L. Wang, H. Li, W. Yan and J. Feng, Synergistic fluoride adsorption by composite adsorbents synthesized from different types of materials—a review, *Front. Chem.*, 2022, **10**, 900660.
13 S. Mushtaq, F. Jamil, M. Hussain, A. Inayat, K. Majeed, P. Akhter, M. S. Khurram, A. Shanableh, Y. M. Kim and Y. K. Park, Utilizing sludge-based activated carbon for targeted leachate mitigation in wastewater treatment, *Environ. Res.*, 2024, 118326.
14 T. Maneerung, J. Liew, Y. Dai, S. Kawi, C. Chong and C. H. Wang, Activated carbon derived from carbon residue from biomass gasification and its application for dye adsorption: kinetics, isotherms and thermodynamic studies, *Bioresour. Technol.*, 2016, **200**, 350–359.
15 H. M. H. Gad, M. M. Hamed, H. A. Eldahab, M. E. Moustafa and S. A. El-Reefy, Radiation-induced grafting copolymerization of resin onto the surface of silica extracted from rice husk ash for adsorption of gadolinium, *J. Mol. Liq.*, 2017, **231**, 45–55.
16 E. Menya, P. W. Olupot, H. Storz, M. Lubwama and Y. Kiros, Production and performance of activated carbon from rice husks for removal of natural organic matter from water: a review, *Chem. Eng. Res. Des.*, 2018, **129**, 271–296.
17 S. Wong, N. Ngadi, I. M. Inuwa and O. Hassan, Recent advances in applications of activated carbon from biowaste for wastewater treatment: a short review, *J. Cleaner Prod.*, 2018, **175**, 361–375.
18 K. K. Kuok, P. C. Chiu, M. R. Rahman, M. Y. Chin and M. K. B. Bakri, Sustainable bamboo and coconut shell activated carbon for purifying river water on Borneo Island, *Waste Manage. Bull.*, 2024, **2**, 39–48.
19 D. Kalderis, A. Seifi, T. K. Trang, T. Tsubota, I. Anastopoulos, I. Manariotis, I. Pashalidis and A. Khataee, Bamboo-derived adsorbents for environmental remediation: A review of recent progress, *Environ. Res.*, 2023, **224**, 115533.
20 L. S. Chan, W. H. Cheung and G. McKay, Adsorption of acid dyes by bamboo derived activated carbon, *Desalination*, 2008, **218**, 304–312.
21 G. Mingjie, *Manual for bamboo charcoal production and utilization*, Bamboo Engineering Research Center, Nanjing Forestry University, China, 2004, pp. 1–24.
22 Y. J. Zhang, Z. J. Xing, Z. K. Duan, M. Li and Y. Wang, Effects of steam activation on the pore structure and surface chemistry of activated carbon derived from bamboo waste, *Appl. Surf. Sci.*, 2014, **315**, 279–286.
23 Y. Wang, X. Wang, X. Wang, M. Liu, Z. Wu, L. Yang, S. Xia and J. Zhao, Adsorption of Pb (II) from aqueous solution to Ni-doped bamboo charcoal, *J. Ind. Eng. Chem.*, 2013, **19**, 353–359.
24 H. Soonmin, N. A. Nordin and R. R. Kannan, A Review of the Bamboo-Based Activated Carbon: Wastewater Treatment & Supercapacitor Device Applications, *Int. J. Eng. Trends Technol.*, 2023, **71**, 69–83.
25 N. Okademi, Effectiveness of Modified Biosand Filters (By Incorporating Bamboo Activated Charcoal, Diatomite, Bone Char, and Steel Wool) in Removal of Fluoride, and *E. Coli* from Water, Doctoral dissertation, University of Eldoret, 2023.
26 C. L. Huang, Y. T. Huang, T. T. Li, C. H. Chiang, C. W. Lou and J. H. Lin, Composite processing and property evaluation of far-infrared/electromagnetic shielding bamboo charcoal/phase change material/stainless steel elastic composite fabrics, *J. Polym. Eng.*, 2016, **36**, 211–220.
27 I. Safarik, K. Horska, K. Pospiskova and M. Safarikova, Magnetically Responsive Activated Carbons for Bio- and Environmental Applications, *Int. Rev. Chem. Eng.*, 2012, **4**, 346–352.
28 P. Kim, N. M. Doss, J. P. Tillotson, P. J. Hotchkiss, M. J. Pan, S. R. Marder, J. Li, J. P. Calame and J. W. Perry, High energy density nanocomposites based on surface-modified $BaTiO_3$ and a ferroelectric polymer, *ACS Nano*, 2009, **3**, 2581–2592.
29 H. Zhou, Z. Jiang and S. Wei, A novel absorbent of nano-Fe loaded biomass char and its enhanced adsorption capacity for phosphate in water, *J. Chem.*, 2013, **1**, 649868.
30 D. S. B. Hashim, J. Y. Liew, J. G. Boon, K. H. Ng and M. S. Shum, Investigation of activated carbon made from Kelantan bamboo as an economical and effective adsorbent for wastewater treatment, *AIP Conf. Proc.*, 2022, **2454**, 1.
31 M. Song, B. Jin, R. Xiao, L. Yang, Y. Wu, Z. Zhong and Y. Huang, the comparison of two activation techniques to prepare activated carbon from corn cob, *Biomass Bioenergy*, 2013, **48**, 250–256.
32 M. T. Hossain, M. M. Hossain, M. H. A. Begum, M. Shahjahan, M. Islam and B. Saha, Magnetite (Fe_3O_4) nanoparticles for chromium removal, *Bangladesh J. Sci. Ind. Res.*, 2018, **53**, 219–224.
33 T. Mahmood, M. Aslam, A. Naeem, T. Siddique and S. U. Din, Adsorption of As (III) from aqueous solution onto iron impregnated used tea activated carbon: Equilibrium, kinetic and thermodynamic study, *J. Chil. Chem. Soc.*, 2018, **63**, 3855–3866.

34 A. Adewuyi, Chemically modified biosorbents and their role in the removal of emerging pharmaceutical waste in the water system, *Water*, 2020, **12**, 1551.
35 C. Anyika, N. A. M. Asri, Z. A. Majid, A. Yahya and J. Jaafar, Synthesis and characterization of magnetic activated carbon developed from palm kernel shells, *Nanotechnol. Environ. Eng.*, 2017, **2**, 1–25.
36 A. N. Fouda, M. D. El Shazly and A. A. Almaqwashi, Facile and scalable green synthesis of N-doped graphene/CNTs nanocomposites via ball milling, *Ain Shams Eng. J.*, 2021, **12**, 1017–1024.
37 K. Liu, L. Xu and F. Zhang, A new preparation process of coal-based magnetically activated carbon, *Chin. J. Geochem.*, 2014, **33**, 173–177.
38 A. Iriel, S. P. Bruneel, N. Schenone and A. F. Cirelli, The removal of fluoride from aqueous solution by a lateritic soil adsorption: kinetic and equilibrium studies, *Ecotoxicol. Environ. Saf.*, 2018, **149**, 166–172.
39 C. M. Carbonaro, D. Chiriu, L. Stagi, M. F. Casula, S. V. Thakkar, L. Malfatti, K. Suzuki, P. C. Ricci and R. Corpino, Carbon dots in water and mesoporous matrix: Chasing the origin of their photoluminescence, *J. Phys. Chem. C*, 2018, **122**, 25638–25650.
40 D. Wang, Z. Wang, Q. Zhan, Y. Pu, J. X. Wang, N. R. Foster and L. Dai, Facile and scalable preparation of fluorescent carbon dots for multifunctional applications, *Engineering*, 2017, **3**, 402–408.
41 J. Wu, L. Zhang, Y. Xia, J. Peng, S. Wang, Z. Zheng and S. Zhang, Effect of microwave heating conditions on the preparation of high surface area activated carbon from waste bamboo, *High Temp. Mater. Processes*, 2015, **34**, 667–674.
42 S. T. Ong, S. P. Yip, P. S. Keng, S. L. Lee and Y. T. Hung, Papaya (Carica papaya) seed as a low-cost sorbent for zinc removal, *Afr. J. Agric. Res.*, 2012, **7**, 810.
43 M. Moyo, L. Chikazaza, B. C. Nyamunda and U. Guyo, Adsorption batch studies on the removal of Pb (II) using maize tassel based activated carbon, *J. Chem.*, 2013, 1–8.
44 Y. H. Huang, Y. J. Shih and C. C. Chang, Adsorption of fluoride by waste iron oxide: The effects of solution pH, major coexisting anions, and adsorbent calcination temperature, *J. Hazard. Mater.*, 2011, **186**, 1355–1359.
45 Y. Liang, X. Xu, F. Yuan, Y. Lin, Y. Xu, Y. Zhang, D. Chen, W. Wang, H. Hu and J. Z. Ou, Graphene oxide additive-driven widening of microporous biochar for promoting water pollutant capturing, *Carbon*, 2023, **205**, 40–53.
46 B. Vijila, E. E. Gladis, J. M. A. Jose, T. M. Sharmila and J. Joseph, Removal of fluoride with rice husk derived adsorbent from agro waste materials, *Mater. Today: Proc.*, 2021, **45**, 2125–2129.
47 R. Sivabalan, S. Rengaraj, B. Arabindoo and V. Murugesan, Cashewnut sheath carbon: A new sorbent for defluoridation of water, *Indian J. Chem. Technol.*, 2003, **10**, 217–222.
48 H. S. Parmar, J. B. Patel, P. Sudhakar and V. J. Koshy, Removal of fluoride from water with powdered corn cobs, *J. Environ. Sci. Eng.*, 2006, **48**, 135–138.
49 R. S. Sathish, N. S. R. Raju, G. S. Raju, G. Nageswara Rao, K. A. Kumar and C. Janardhana, Equilibrium and kinetic studies for fluoride adsorption from water on zirconium impregnated coconut shell carbon, *Sep. Sci. Technol.*, 2007, **42**, 769–788.
50 G. Alagumuthu and M. Rajan, Equilibrium and kinetics of adsorption of fluoride onto zirconium impregnated cashew nut shell carbon, *Chem. Eng. J.*, 2010, **158**, 451–457.
51 G. Alagumuthu and M. Rajan, Kinetic and equilibrium studies on fluoride removal by zirconium (IV): Impregnated groundnut shell carbon, *Hem. Ind.*, 2010, **64**, 295–304.
52 A. Mohammad and C. B. Majumder, Removal of fluoride from synthetic waste water by using "bio-adsorbents", *Int. J. Res. Eng. Technol.*, 2014, **3**, 776–785.
53 D. S. Dwivedi Shubha, M. P. Mondal Prasenjit and B. C. Balomajumder Chandrajit, Removal of fluoride using Citrus limetta in batch reactor: kinetics and equilibrium studies, *Res. J. Chem. Sci.*, 2014, **4**, 50–58.
54 R. Jha, U. Jha, R. K. Dey, S. Mishra and S. K. Swain, Fluoride sorption by zirconium (IV) loaded carboxylated orange peel, *Desalin. Water Treat.*, 2015, **53**, 2144–2157.
55 V. Veeraputhiran and G. Alagumuthu, Adsorption kinetics and thermodynamics of fluoride onto Phyllanthus emblica based thermally activated carbon, *Int. J. ChemTech Res.*, 2012, **4**, 165–174.
56 K. P. Piyush, P. Madhurima and S. Rekha, Defluoridation of water by a biomass: Tinospora cordifolia, *J. Environ. Prot.*, 2012, **3**, 1–7.
57 S. Dwivedi, P. Mondal and C. Balomajumder, Bioadsorption of fluoride by Ficusreligiosa (Peepal Leaf Powder): optimization of process parameters and equilibrium study, *Res. J. Chem. Sci.*, 2014, **2231**, 606X.